Catalysis Letters (2018) 148:1228–1235
https://doi.org/10.1007/s10562-018-2333-4

The Keggin Structure: An Important Factor in Governing NH_3–SCR Activity Over the V_2O_5–MoO_3/TiO_2 Catalyst

Rui Wu[1] · Ningqiang Zhang[1] · Xiaojun Liu[3] · Lingcong Li[1] · Liyun Song[1] · Wenge Qiu[1] · Hong He[1,2]

Received: 2 December 2017 / Accepted: 25 January 2018 / Published online: 23 February 2018

Abstract

Heteropolyacids and their salts have been effectively used in selective catalytic reduction because of the Keggin structure and extraordinarily strong acidity. Catalysts with and without the Keggin structure were synthesized to further investigate the effects of heteropolyoxometallate on low temperature NH_3–SCR. XRD, BET, Raman, H_2–TPR, NH_3–TPD, FT-IR, and SO_2–TPD techniques were used to characterize the physicochemical characteristics of the catalysts. Results indicate that catalysts with the Keggin structure had more surface Brönsted and Lewis acid sites, and these catalysts had significantly improved performances in the SCR reaction and in SO_2 poisoning resistance.

Graphical Abstract

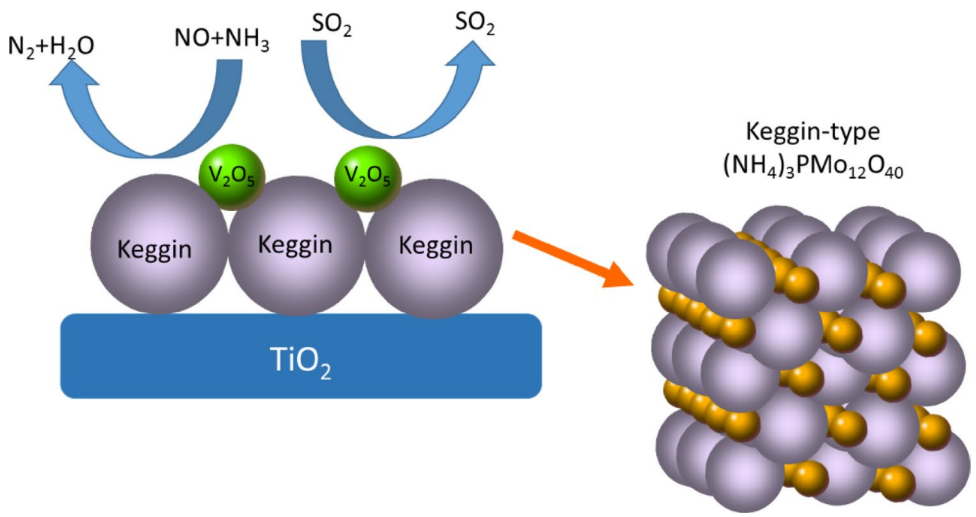

Keywords SCR catalyst · Ammonium heteropolyacid salt · Keggin structure

Rui Wu and Ningqiang Zhang have contributed equally.

✉ Hong He
hehong@bjut.edu.cn

[1] Laboratory of Catalysis Chemistry and Nanoscience, Department of Chemistry and Chemical Engineering, College of Environmental and Energy Engineering, Beijing University of Technology, Beijing 100124, People's Republic of China

[2] Collaborative Innovation Center of Electric Vehicles in Beijing, Beijing 100081, People's Republic of China

[3] College of Chemistry, Chemical Engineering and Materials Science, Institute of Molecular and Nano Science, Shandong Normal University, Jinan 250014, Shandong, People's Republic of China

1 Introduction

Selective catalytic reduction (SCR) catalysts have been the subject of intense research interest and are a major technology used to control NO_x emission. In recent decades, commercial V_2O_5–WO_3 (MoO_3)/TiO_2 catalysts have been widely used, have high activity, and are quite resistant to SO_2 [1, 2]. However, NH_3–SCR over these catalysts can only be operated in a narrow temperature window of 300–400 °C, and the phase of TiO_2 can be transformed from anatase to rutile at elevated temperature; this phase transformation results in a loss of SCR activity [3]. Great efforts have been made to improve the low-temperature activity of NH_3–SCR over catalysts, such as CeO_2/TiO_2, MnO_x/Al_2O_3, CuO–CeO_2/TiO_2, and Mn–Ce/TiO_2, which have been developed and used as SCR catalysts [4–6]. The main problem with these catalysts is SO_2 resistance because SO_2 oxidation that occurs with H_2O results in the formation of ammonium sulfates, which inhibit SCR activity of the catalysts at temperatures below 300 °C [7–10].

Heteropolyacids (HPAs) and their salts have attracted much interest because of their strong acidity, redox properties and unique structures. Of the many structural types of HPAs, the majority used in catalytic applications are Keggin HPAs, such as $H_3PW_{12}O_{40}$, $H_4SiW_{12}O_{40}$, and $H_3PMo_{12}O_{40}$ because of their stronger acidity, higher thermal stability, and easier availability [11, 12]. It has been reported that Keggin HPAs have excellent NO adsorption behavior and that rapid heating can cause absorbed NO to be decomposed into N_2 [13–15]. Other research has shown that Pt loaded on Keggin HPAs can enhance the activity of NO reduction [16]. Recently developed HPAs and their salts have attracted much attention because of their use for SCR. Yoshimoto et al. [17] used a mixture of Na-ZSM-5 and Pd/$H_3PW_{12}O_{40}$/SiO_2 as a catalyst for the selective reduction of NO using aromatic hydrocarbons and reported that the catalyst had high activity for NO reduction. Putluru et al. [18] developed heteropolyacid-promoted V_2O_5/TiO_2 catalysts for NH_3–SCR, and they found that the catalysts had excellent alkali deactivation resistance. Their results suggested that the SCR activity of heteropolyacid-promoted catalysts is much higher than that of ordinary SCR catalysts. Additionally, many reports have shown that the CeO_2/$H_3PW_{12}O_{40}$ catalyst has enhanced SCR activity and SO_2 poisoning resistance because SO_2 cannot gain access into the secondary structure, but NO_x molecules can enter the structure [19–21].

However, there are relatively few studies comparing the effects of heteropolyacids and the oxide phase on the SCR reaction. Because heteropolyacids have more P atoms than the common oxide SCR catalyst, it has been reported that a small quantity of P_2O_5 and H_3PO_4 can enhance SCR catalytic performance [22]. On the other hand, heteropolymolybdates are easily generated if PO_4^{3-} and MoO_4^{2-} are both present in solution. It is not clear that whether the improved SCR performance is caused by the addition of phosphorus or by the unique Keggin structure of heteropolyacids and their salts. Two groups of catalysts with and without the Keggin structure were prepared via simple impregnation, and the activities of these catalysts for NH_3–SCR were evaluated to investigate the effects of the Keggin structure on a catalyst used for a low SCR reaction. XRD, TEM, H_2–TPR, NH_3–TPD, and FT-IR techniques were used to characterize the physicochemical properties of the samples.

2 Experimental Methods

2.1 Catalyst Preparation

Two kinds of catalysts were prepared using the impregnation method, and the main chemical compositions were the same. The compositions were calculated so that $(NH_4)_3PMo_{12}O_{40}$ loading was 20 wt% and V_2O_5 loading was 1 wt%.

The catalysts with an oxide phase were prepared via multiple impregnation methods to avoid generating the Keggin structure. $(NH_4)_6Mo_7O_{24}$ (11.5 g, Fuchen, China, 99%) was dissolved in 100 mL of distilled water for 20 min. TiO_2 anatase powder (Xinhua, China, 99%) was impregnated with the precursor solution and stirred at 80 °C for 5 h and then dried at 120 °C for 3 h. The solid was ground into a powder and calcined at 400 °C for 5 h. MoO_3/TiO_2 powder was obtained. Next, 0.6 g of $NH_4H_2PO_4$ (Fuchen, China, 99%) was dissolved in 100 mL of distilled water, and the MoO_3/TiO_2 powder was impregnated. Desiccation and calcination conditions were the same as above. The obtained sample was denoted Cat-A. Then, 0.6 g of NH_4VO_3 (Fuchen, China, 99%) was added to a solution of oxalic acid; the weight of $H_2C_2O_4{\cdot}2H_2O$ (Fuchen, China, 99%) was double that of NH_4VO_3. Cat-A powder (9.9 g) was impregnated in the above solution and stirred at 80 °C for 5 h. Desiccation and calcination conditions were the same as above, and the obtained catalyst was denoted Cat-A-V.

Catalysts with the Keggin structure were also prepared using an impregnation method. $NH_4H_2PO_4$ and $(NH_4)_6Mo_7O_{24}$ were dissolved in distilled water and pH of the solution was adjusted to a value of about 1. TiO_2 anatase powder was impregnated with the precursor solution. After drying and calcining using the above conditions, the obtained sample was denoted Cat-B. After loading V_2O_5 with the above conditions, the sample was denoted Cat-B-V.

2.2 Catalyst Characterization

Powder X-ray diffraction (XRD) measurements were made using a Bruker D-8 system with Cu radiation (λ = 0.15418 nm) at 40 kV and 100 mA. To determine the crystal structure, the experimental data were collected in the 2θ range of 10°–80° with a step of 0.02°/0.3 s.

Micromeritics ASAP 2020 automated gas sorption system was used to obtain N_2 adsorption–desorption isotherms at − 196 °C. The Brunauer–Emmett–Teller (BET) model was used to evaluate the specific surface areas of the samples from these isotherms. X-ray fluorescence (XRF) measurements (Magix PW2403, Netherlands) were used to analyze the elemental composition of the catalysts.

H_2–temperature programmed reduction (H_2–TPR) was conducted over a chemisorption analyzer (AUTOSORB-1C, American). Before the H_2–TPR experiments, 50 mg of catalyst were pretreated in pure N_2 at 350 °C for 60 min and cooled to 100 °C. H_2–TPR runs were carried out in a flow of 5 vol% H_2/He (30 mL/min) from 40 to 900 °C at a heating rate of 10 °C/min.

Temperature-programmed desorption of ammonia (NH_3–TPD) and sulfur dioxide (SO_2–TPD) were used to investigate the total acidities of the catalysts on a chemisorption instrument equipped with a thermal conductivity detector (Quantachrome Chem BET Pulsar TPR/TPD, American). Before the experiment, the catalysts were pretreated in pure He at 400 °C for 60 min. The samples were then saturated with 5% NH_3/He or SO_2/He at a flow rate of 30 mL/min for about 30 min. The samples were heated from 50 to 900 °C with a heating rate of 10 °C/min to carry out desorption.

FT-IR measurements were performed on a Nicolet 6700 FTIR spectrometer coupled with ZnSe windows at 4 cm^{-1} resolution with 32 co-added scans. In the DRIFT cell, catalysts were pretreated at 300 °C in a He environment for 30 min, and then cooled to room temperature in He. The sample was heated, and DRIFT spectra were collected at 200 °C.

A Raman Spectrometer (JY T64000, American) with a 532 nm wavelength excitation laser was used to measure the micro-Raman spectra of different areas of the grown mullite crystal. Pure powder supported on a sheet of glass was used without any pretreatment.

A high-resolution Raman spectrometer (Renishaw inVia Reflex) was used to record in situ Raman spectra at five laser excitations (785, 633, 532, 325, and 244 nm). The 532-nm line was used to record the Raman spectra. The samples (about 20 mg of loose powder) were loaded in an in situ cell with a quartz window; and the samples were treated using desired temperatures and gas flows. The samples were heated to 250 °C under an atmosphere of N_2 at a total flow rate of 50 mL/min for 30 min to remove any adsorbed impurities. Then, 500 ppm NO/N_2, 500 ppm NH_3/N_2, and 6% O_2 were added to simulate SCR conditions. Finally, NO, NH_3, and O_2 were cut off and N_2 was purged. During every stage, the spectra were recorded.

2.3 Activity Test

SCR performance measurements were taken using a fixed bed quartz reactor (9 mm i.d.) with 0.4 mL of catalysts (40–60 mesh). The gas flow was measured using mass flow meters. The concentrations of simulated gases were as follow: 1000 ppm NO, 1000 ppm NH_3, 5% O_2, 5% water vapor, and 350 ppm SO_2 with a balance of N_2. The space velocity was 40,000 h^{-1}. The concentrations of NO and NH_3 were continuously measured using a Thermo Scientific 17i NO_x chemiluminescence analyzer. N_2O was monitored using a Bruker Tensor 27 FTIR spectrometer. The reaction system was maintained at each reaction temperature for 30 min before analysis. The equations to calculate NO_x conversion and N_2 selectivity were as follows:

$$\text{NO conversion}\,(\%) = \frac{[\text{NO}]_{\text{in}} - \left([\text{NO}]_{\text{out}} + [\text{NO}_2]_{\text{out}}\right)}{[\text{NO}]_{\text{in}}} \times 100\% \quad (1)$$

$$N_2\ \text{selectivity}\,(\%) = \left(1 - \frac{[\text{NO}_2]_{\text{out}} + 2[\text{N}_2\text{O}]_{\text{out}}}{[\text{NH}_3]_{\text{in}} + [\text{NO}]_{\text{in}} - [\text{NH}_3]_{\text{out}} - [\text{NO}]_{\text{out}}}\right) \times 100\% \quad (2)$$

3 Results and Discussion

To study the effects of the Keggin structure, it is necessary to confirm the crystalline phase of the materials. XRD patterns of the samples are shown in Fig. 1. All of the catalysts exhibited the characteristic pattern of TiO_2-anatase

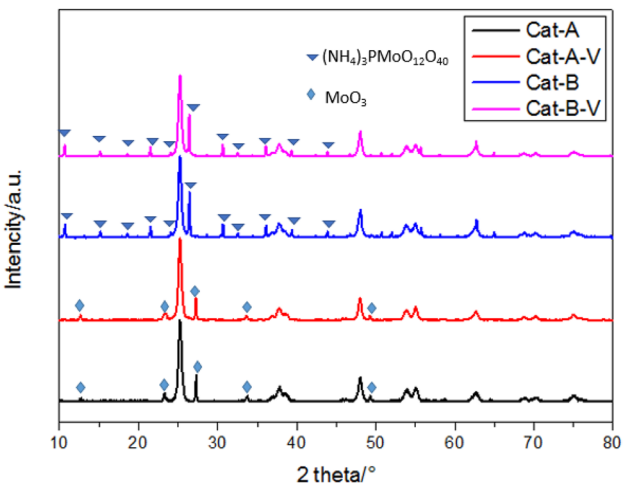

Fig. 1 XRD patterns of Cat-A and Cat-B

peaks (PDF-JCPDS-65-5724) [23] with diffraction lines at $2\theta = 25.2°$, 37.7°, 48.1°, 53.8°, 55.0°, and 62.7°. For Cat-A and Cat-A-V, the characteristic diffraction peaks at 11.5°, 24.5°, 27.5°, and 34.5° can be assigned to orthorhombic MoO_3 [24]. In the XRD profile of Cat-B and Cat-B-V, peaks at 10.5°, 15.5°, 26.5°, and 30.5° were found, and can be indexed to Keggin-type $(NH_4)_3PMoO_{12}O_{40}$ (PDF-JCPDS-43-0315) [25]; no peaks corresponding to MoO_3 were observed. Peaks corresponding to P_2O_5 and V_2O_5 were not be detected because these species were well dispersed on the surface of TiO_2. Therefore, the XRD results show that two groups of materials have different crystalline structures, as designed.

Raman spectroscopy is a sensitive technique for studying supported metal oxide structures. Raman spectroscopic investigation was conducted to obtain further confirmation of the two materials. The Raman spectra of the two materials are shown in Fig. 2, and as seen in Fig. 2, the Raman spectra in the range 700–1100 cm^{-1} under ambient conditions provide evidence for the different structures. For Cat-A and Cat-A-V, the peaks at 817 and 993 cm^{-1} can be attributed to the Mo–O–Mo symmetric stretch and the Mo=O vibration, respectively [23–26]. For Cat-B and Cat-B-V, there are three intense peaks that can be attributed to the Keggin anion. The peak at 900 cm^{-1} can be assigned to the Mo–O–Mo vibration, and the peaks at 989 and 1000 cm^{-1} can be attributed to the Mo–O vibration in the Keggin anion [26, 27]. The results further confirm that the materials have different structures.

Table 1 shows the XRF elemental analysis results and the BET specific surface areas for all of the samples. The chemical compositions of the four samples were nearly identical and were similar to the theoretical design. Furthermore, the BET specific surface areas of the four catalysts were the same and were all approximately 53 m^2/g.

Figure 3 provides a comparison of NO conversion over each of the catalysts. NO conversions were significantly different for the four catalysts over the temperature range of 160–350 °C. Cat-A had poor SCR activity below 250 °C and more than 90% NO conversion over the range of 280–350 °C. For Cat-B, NO conversion reached about 90% over the range of 270–350 °C, and this was slightly better than that for Cat-A. After loading V_2O_5, the NO conversions over the two catalysts were obviously improved. Compared to Cat-A-V, the SCR activity was significantly enhanced at low temperature

Table 1 Compositions and BET surface areas of Cat-A and Cat-B

Catalysts	Element content (wt%)				S_{BET} (m^2 g)
	Ti	Mo	P	V	
Cat-A	48.5	11.9	0.4	–	52
Cat-B	48.8	11.5	0.4	–	53
Cat-A-V	48.2	11.6	0.4	0.5	53
Cat-B-V	48.0	11.8	0.4	0.5	52

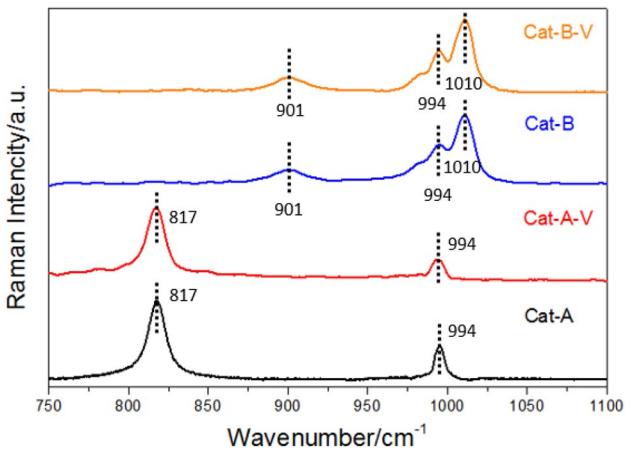

Fig. 2 Raman spectra of Cat-A and Cat-B

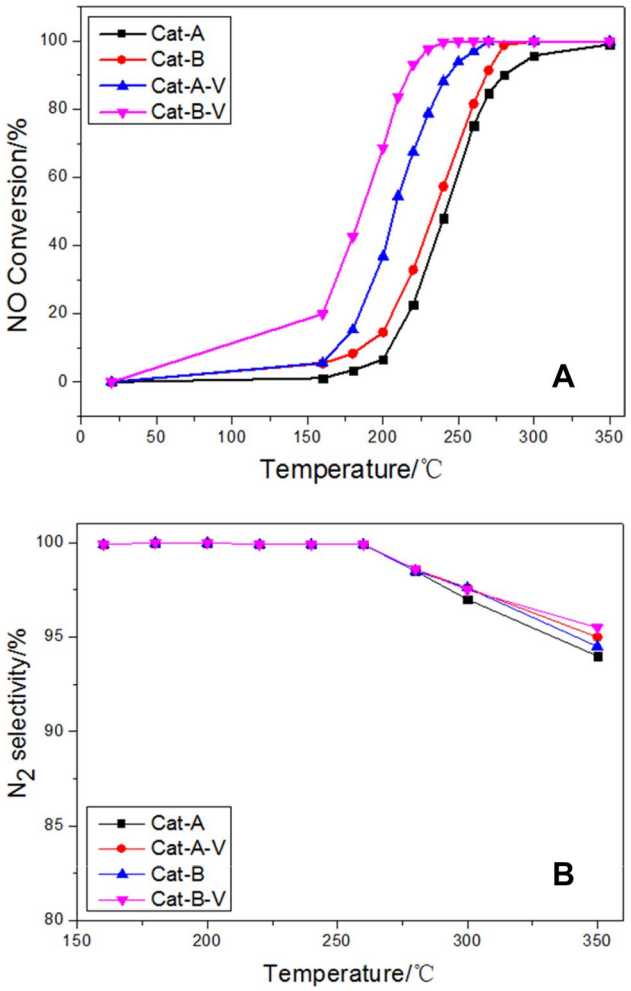

Fig. 3 NO conversion (**a**) and N_2 selectivity (**b**) of NH_3–SCR over the catalysts. Reaction conditions: $[NO] = [NH_3] = 1000$ ppm, $[O_2] = 5\%$, $[SO_2] = 350$ ppm, water vapor = 3%, N_2 balance, and GHSV = 40,000 h^{-1}

over Cat-B-V, and the NO conversion was about 93% at 220 °C. In contrast, the NO conversion over Cat-A-V was only 67% at the same temperature. In brief, the Cat-B and Cat-B-V catalysts, which each had a Keggin structure, exhibited much higher NO conversion than the Cat-A and Cat-A-V catalysts, which each had an oxide phase, and this suggests that the SCR performance of the catalysts was largely affected by the Keggin structure. The N_2 selectivities of all of samples over the range of 160–350 °C are shown in Fig. 3b. All of the catalysts had similar N_2 selectivity, and over 90% N_2 selectivity was obtained over the range of 160–350 °C.

To study the stability of the Keggin structure in SCR conditions, in situ Raman spectra were collected at 250 °C under the following conditions: first, N_2 was used to purge the surface; second, 500 ppm NO/N_2, 500 ppm NH_3/N_2, and 6% O_2 were added to simulate SCR conditions; finally, N_2 was used to purge the adsorption of NO and NH_3. Figure 4 shows the in situ Raman spectra of Cat-B-V. The characteristic peaks of the Keggin structure were observed at 250 °C and with present of NH_3 and NO, the peaks had not any shift. After purging with N_2, the peaks were unchanged. The result indicated that there was no structural perturbation resulting from the temperature and reaction gas and the Keggin structure was stable in SCR conditions.

The reducibility of all of the catalysts was examined using H_2–TPR, and the results are summarized in Fig. 5 and Table 2. The TPR profile of Cat-A shows two peaks centered at 460 and 800 °C, which correspond, respectively, to the reduction of Mo^{6+} into Mo^{4+} and that of Mo^{4+} into metallic Mo [6, 28]. The TPR profile of Cat-B has three peaks; the peaks at 440 and 510 °C can be attributed to the reduction from Mo^{6+} to Mo^{4+}, and the peak at 720 °C can be assigned to the reduction

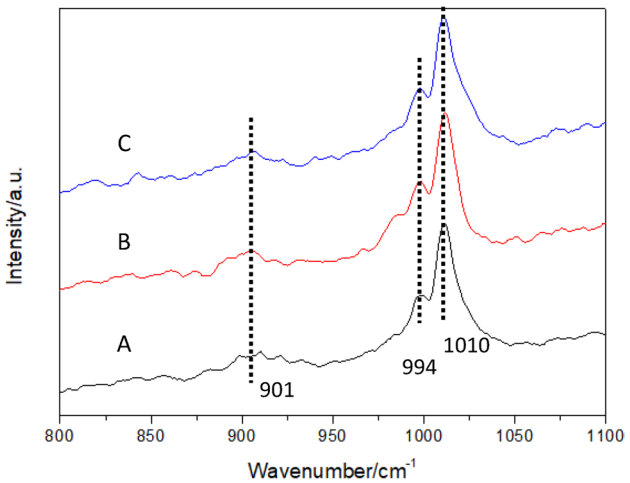

Fig. 4 In situ sequential Raman spectra of Cat-B-V at 250 °C under various atmospheres: **a** the catalyst was treated with N_2; **b** then NO + NH_3 + O_2 was added; **c** NO + NH_3 + O_2 was stopped, and the catalyst was treated with N_2 again

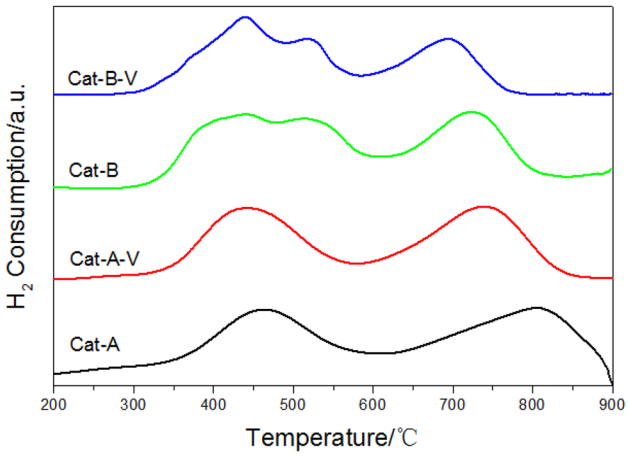

Fig. 5 H_2–TPR profiles of the catalysts

from Mo^{4+} to Mo [29, 30]. For Cat-B, it can be noted that the positions of the reduction peaks were slightly shifted to lower temperature, but the H_2 consumption (Table 2) was similar to that of Cat-A. TPR profiles of Cat-A-V and Cat-B-V have similar peaks as Cat-A and Cat-B, respectively. However, the reduction peaks for Cat-A-V and Cat-B-V are also shifted to lower temperature. Also, the H_2 consumption increased as compared to the Cat-A and Cat-B, and this shows that V_2O_5 markedly improved the redox ability of the catalyst. Reduction peaks for V species were not clearly detected in the TPR profiles because of the low concentration of V in the catalysts and because the reduction peaks of V species might be overlapped with the reduction peaks of Mo species.

In an SCR reaction, it is important to adsorb and activate NH_3 molecules on the surface of a catalyst. Adsorption and desorption of NH_3 are greatly influenced by the surface acidity of SCR catalysts [31]. The acidity of the catalysts used in this study was measured via the NH_3–TPD method. NH_3–TPD profiles of all of the catalysts are shown in Fig. 6. For all of the catalysts, a broad NH_3-desorption pattern is found from 50 to 700 °C. The total amount of adsorbed ammonia was calculated in terms of the desorption area of the TPD curve. The peaks in the NH_3–TPD profile at low temperature can be assigned to NH_3 desorption at the weak acidic sites, and the peaks at high temperature can be assigned to NH_3 desorption at strong acidic sites [23, 32]. The peak intensities for Cat-B and Cat-B-V were obviously higher than those for Cat-A and Cat-A-V, and this indicates that Cat-B and Cat-B-V (with the Keggin structure) had more acidic sites than Cat-A and Cat-A-V. NH_3 desorption peaks at high temperature (above 400 °C) for Cat-B

Table 2 H_2–TPR results

Catalysts	Cat-A	Cat-A-V	Cat-B	Cat-B-V
Hydrogen consumption (mmol/g)	3.4	7.0	3.1	6.8

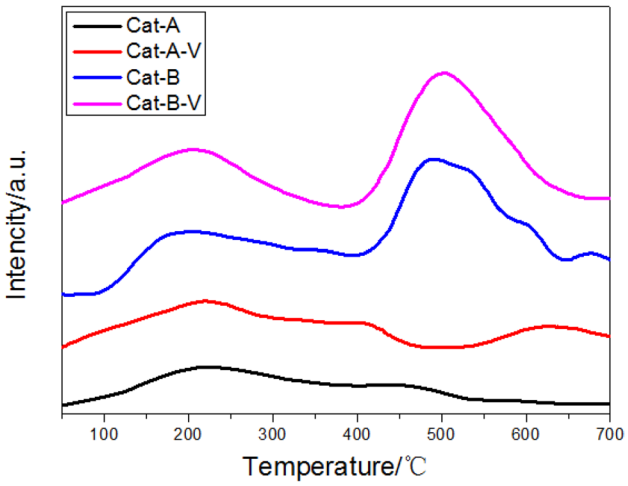

Fig. 6 NH_3–TPD profiles of the catalysts

and Cat-B-V were broader than the peaks at low temperature, and this suggests that there were more sites with strong acidity than with week acidity. In contrast, this phenomenon was not observed with Cat-A and Cat-B. As discussed above, the activities for SCR reactions over the Cat-B and Cat-B-V catalysts were much higher than those over the Cat-A and Cat-B catalysts. It is suggested that the superior surface acidity of Cat-B and Cat-B-V dominates the activity of SCR over the catalysts. It should be noted that the NH_3–TPD experiment was not capable of discriminating between Brönsted and Lewis acid sites, and thus a different method was needed to acquire more information regarding the surface acidity [32].

FT-IR measurements of pyridine adsorption were used to determine the acidic properties of the catalysts. As shown in Fig. 7, the FT-IR spectra of pyridine adsorption were measured over the range of 1400–1600 cm^{-1} for each of the catalysts. Three peaks at 1450, 1490, and 1538 cm^{-1} were observed. The IR absorptions at 1538 and 1450 cm^{-1}

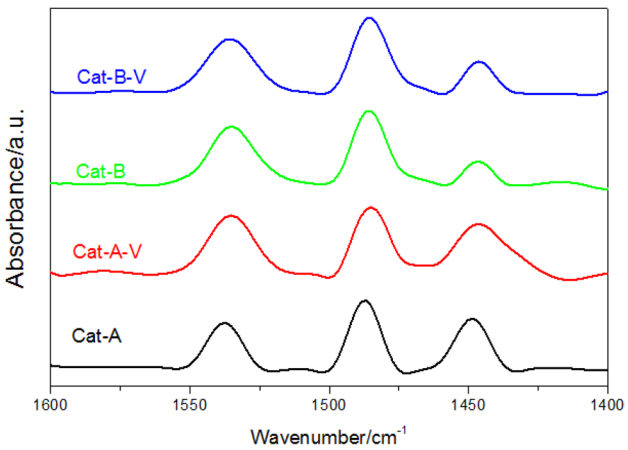

Fig. 7 FT-IR spectra of adsorbed pyridine on the catalysts at 200 °C

are known to correspond to pyridine adsorbed on Brönsted acid sites and Lewis acid sites, respectively [33, 34]. The bond intensities of Cat-A and Cat-A-V at 1538 cm^{-1} were similar to the intensity of the peak at 1450 cm^{-1}, illustrating that the amounts of Brönsted acid and Lewis acid sites were almost the same. In contrast, the bond intensities of Cat-B and Cat-B-V at 1538 cm^{-1} were stronger than the absorption at 1450 cm^{-1}, indicating that there were more Brönsted acid sites than Lewis acid sites over the Cat-B and Cat-B-V materials. It is important to have Brönsted and Lewis acid sites for SCR of NO with NH_3, but which of these kinds of acids is predominantly important is still under debate. In combining the NH_3–TPD and FT-IR results, the conclusion is drawn that the Keggin structure provides more Brönsted and Lewis acid sites, and this is an important factor in increasing SCR activity over these catalysts.

It is well known that SO_2 can be oxidized to SO_3 over supported V_2O_5 catalysts and that SO_3 reacts with NH_3 in the presence of H_2O to produce ammonium bisulfate (ABS, NH_4HSO_4) at low temperature. Adding MoO_3 to SCR catalysts can enhance SO_2 [34]. It has been reported that NO and NH_3 can access the space of the Keggin structure and that they can substitute for H_2O linkages in the secondary structure. However, SO_2 cannot enter the Keggin structure. To investigate the effects of H_2O and SO_2 on the activities of the catalysts with and without the Keggin structure, the effects of H_2O and SO_2 on the activities of Cat-A-V and Cat-B-V were investigated at 250 °C, and the results are shown in Fig. 8. As seen in Fig. 8, it could be found that after H_2O and SO_2 gases were introduced into the SCR reaction system, NO_x conversion over the Cat-A-V catalyst decreased from 100 to 61% in 7 h. In the case of the Cat-B-V catalyst, although NO conversion also decreased, it was still 83% at

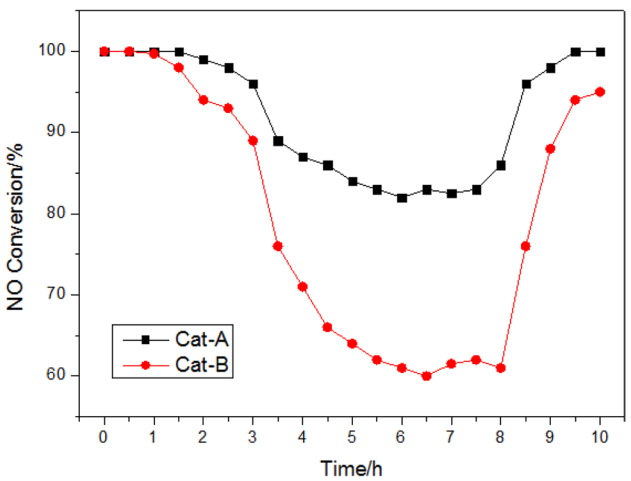

Fig. 8 Effects of H_2O and SO_2 on NO conversion over Cat-A-V and Cat-B-V. Reaction conditions: temperature = 250 °C, [NO] = [NH_3] = 1000 ppm, [O_2] = 5%, [SO_2] = 1000 ppm, GHSV = 40,000 h^{-1}, and [H_2O] = 10%

8 h, and this was much higher than that over the Cat-A-V catalyst. When the H_2O and SO_2 flows were cut off, NO conversion over Cat-A-V was 95% in 2 h. However, over Cat-B-V, NO conversion was 100% in 1.5 h. This suggests that the Cat-B-V catalyst has better H_2O and SO_2 resistance. Because of this, the SO_2 molecule cannot enter the Keggin structure; thus, oxidation and adsorption of SO_2 over Cat-B-V was suppressed, and the Keggin structure restrained competitive adsorption of SO_2 and NO.

SO_2–TPD was measured for Cat-A-V and Cat-B-V to further understand SO_2 resistance that results from the Keggin structure. The SO_2–TPD patterns are shown in Fig. 9. There were two shoulder peaks around 600 and 650 °C for Cat-A-V, and one shoulder peak appeared around 450 °C for Cat-B-V. These peaks were assigned to the SO_2 chemisorbed desorption on the surface of the catalysts [35]. It is clear that Cat-B-V showed lower SO_2 adsorption properties. Furthermore, Cat-B-V had a lower temperature shift signal, and this suggests SO_2 adsorption was inhibited. These results demonstrate that the Keggin structure can reduce SO_2 adsorption and lead to improved SO_2 poisoning resistance.

4 Conclusion

The effect of the Keggin structure on the low-temperature SCR reaction was investigated in this paper. For SCR with NH_3, catalysts that have the Keggin structure had higher activity than catalysts without the Keggin structure, and the Keggin structure was stable under SCR conditions. The two kinds of catalysts had similar chemical compositions, surface areas, and reducibility; however, the catalysts with the Keggin structure had more Brönsted and Lewis acid sites, and these increased the activity of NH_3–SCR over the catalyst. In addition, the catalysts that had the Keggin structure also had improved resistance to SO_2 and H_2O poisoning because SO_2 adsorption was reduced by the Keggin structure and led to suppressing SO_2 poisoning.

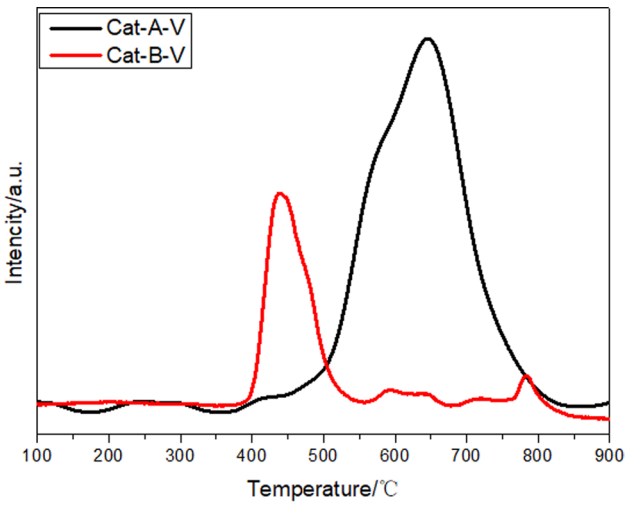

Fig. 9 SO_2–TPD patterns for Cat-A-V and Cat-B-V

Acknowledgements The work was supported by the National Key R&D Program of China (2017YFC0210303-02) and the National Natural Science Foundation of China (201577005, 21507075). The authors thank Ran Liu from Shiyanjia lab for assistance of BET and NH_3–TPD analysis (http://www.Shiyanjia.com).

References

1. Busca G, Lietti L, Ramis G, Berti F (1998) Appl Catal B 18:1–36
2. Amiridis MD, Duevel RV, Wachs IE (1999) Appl Catal B 20:111–122
3. Pârvulescu VI, Grange P, Delmon B (1998) Catal Today 46:233–316
4. Peng Y, Li K, Li J (2013) Appl Catal B 140–141:483–492
5. Jin R, Liu Y, Wang Y, Cen W, Wu Z, Wang H, Weng X (2014) Appl Catal B 148:582–588
6. Mejri I, Ayari F, Mhamdi M, Delahay G, Ksibi Z, Ghorbel A (2016) Microporous Mesoporous Mater 220:239–246
7. Zhang X, Li Z, Zhao J, Cui Y, Tan B, Wang J, Zhang C, He G (2017) Korean J Chem Eng 34:2065–2071
8. Liu Z, Zhu J, Zhang S, Ma L, Woo SI (2014) Catal Commun 46:90–93
9. Yu Y, Wang J, Chen J, Meng X, Chen Y, He C (2014) Ind Eng Chem Res 53:16229–16234
10. Jiang BQ, Wu ZB, Liu Y, Lee SC, Ho WK (2010) J Phys Chem C 114:4961–4965
11. Kozhevnikov IV (1998) Chem Rev 98:171–198
12. Mizuno N, Misono M (1998) Chem Rev 98:199–218
13. Yang RT, Chen N (1994) Ind Eng Chem Res 33:825–831
14. Bélanger R, Moffat JB (1998) Catal Today 40:297–306
15. Heylen S, Smeekens S, Kirschhock C, Parac-Vogt T, Martens JA (2010) Energy Environ Sci 3:910–916
16. Vaezzadeh K, Petit C, Pitchon V (2002) Catal Today 73:297–305
17. Yoshimoto R, Ninomiya T, Okumura K, Niwa M (2007) Appl Catal B 75:175–181
18. Putluru SSR, Jensen AD, Riisager A, Fehrmann R (2011) Catal Sci Technol 1:631–637
19. Song Z, Zhang Q, Ning P, Fan J, Duan Y, Liu X, Huang Z (2016) J Taiwan Inst Chem Eng 65:149–161
20. Weng X, Dai X, Zeng Q, Liu Y, Wu Z (2016) J Colloid Interface Sci 461:9–14
21. Song Z, Zhang Q, Ma Y, Liu Q, Ning P, Liu X, Wang J, Zhao B, Huang J, Huang Z (2017) J Taiwan Inst Chem Eng 71:277–284
22. Kamata H, Takahashi K, Odenbrand CI (1998) Catal Lett 53:65–71
23. Maqbool MS, Pullur AK, Ha HP (2014) Appl Catal B 152:28–37
24. Ballarini N, Candiracci F, Cavani F, Degrand H, Dubois J-L, Lucarelli G, Margotti M, Patinet A, Pigamo A, Trifiro F (2007) Appl Catal A 325:263–269

25. Jing F, Katryniok B, Bordes-Richard E, Paul S (2013) Catal Today 203:32–39
26. Bajuk-Bogdanović D, Uskoković-Marković S, Hercigonja R, Popa A, Holclajtner-Antunović I (2016) Spectrochim Acta A 153:152–159
27. Demirel B, Fang S, Givens EN (2000) Appl Catal A 201:177–190
28. Liu Z, Zhang S, Li J, Ma L (2014) Appl Cataly B 144:90–95
29. Damyanova S, Cubeiro ML, Fierro JLG (1999) J Mol Catal A 142:85–100
30. Spojakina AA, Kostova NG, Sow B, Stamenova MW, Jiratova K (2001) Catal Today 65:315–321
31. Sultana A, Sasaki M, Hamada H (2012) Catal Today 185:284–289
32. Yang R, Huang H, Chen Y, Zhang X, Lu H (2015) Chin J Catal 36:1256–1262
33. Liu Y, Ma X, Wang S, Gong J (2007) Appl Catal B 77:125–134
34. Chang H, Li J, Chen X, Ma L, Yang S, Schwank JW, Hao J (2012) Catal Commun 27:54–57
35. Kwon DW, Park KH, Hong SC (2016) Chem Eng J 284:315–324